Scilight

Intelligence & Control
https://www.sciltp.com/journals/ic

Article

Check for updates

Adaptive Fixed-Time Sliding Mode Tracking Control of Underactuated AUVs with Flexible Prescribed Performance

Gaofeng Fan, Ying Zhao * and Shuanghe Yu

College of Marine Electrical Engineering, Dalian Maritime University, Dalian 116026, China
* Correspondence: yingz@dlmu.edu.cn

How To Cite: Fan, G.; Zhao, Y.; Yu, S. Adaptive Fixed-Time Sliding Mode Tracking Control of Underactuated AUVs with Flexible Prescribed Performance. *Intelligence & Control* **2026**, *2*(2), 4. https://doi.org/10.53941/ic.2026.100007

Received: 21 April 2026
Revised: 14 June 2026
Accepted: 17 June 2026
Published: 30 June 2026

Abstract: This paper proposes a fixed-time nonsingular terminal sliding mode control (FXTNTSMC) method for underactuated autonomous underwater vehicles (AUVs) under uncertain dynamics and flexible prescribed performance. To address the inherent limitation of conventional prescribed performance control (PPC), the rigid performance bounds that may induce system instability under large disturbances, a flexible PPC strategy is proposed. This approach incorporates a risk monitoring mechanism that proactively predicts the tendency of the tracking error to violate performance constraints and dynamically adjusts the performance boundaries, thereby preserving transient performance while circumventing controller singularity. Furthermore, a FXTNTSMC law is designed to guarantee the tracking error can achieve a bounded region within a fixed time independent of initial conditions. An improved adaptive radial basis function neural network is employed for online approximation of the lumped disturbance, which consists of both uncertain dynamics and unknown external disturbances. Finally, a simulation shows that the superiority of the FXTNTSMC scheme in terms of tracking accuracy and convergence rate.

Keywords: underactuated autonomous underwater vehicles; fixed-time nonsingular terminal sliding mode; flexible prescribed performance control

1. Introduction

The application of autonomous underwater vehicles (AUVs) has become prevalent in key fields, particularly in military operations, ocean resource surveys, and high-precision seabed mapping [1–3]. These diverse missions have spurred significant research interest in advanced motion control methodologies for AUVs, generating a substantial body of academic work on fundamental topics including trajectory tracking, target pursuit, and efficient path planning [4–6]. However, the physical design of most AUVs results in an underactuated configuration. This inherent underactuation, combined with the complex hydrodynamic environment, greatly increases the challenge of designing effective and robust tracking controllers. Consequently, developing reliable trajectory tracking control strategies for underactuated AUV remains a noteworthy, challenging, and practically significant research focus.

It is noteworthy that the uncertain dynamics inherent to underactuated AUV systems and external disturbances further intensify the challenges in control strategy design [7,8]. During actual marine operations, underactuated AUV is inevitably subject to time-varying external environmental forces, such as ocean currents and waves, which act as additional disturbances. Moreover, obtaining precise values for the hydrodynamic parameters of underactuated AUVs is extremely difficult; typically, only approximations derived from experiments or computational fluid dynamics are available. These combined factors can severely degrade tracking performance, induce instability, and even lead to system failure, demanding control strategies with exceptional robustness [9,10]. Due to its inherent invariance to matched model uncertainties and external disturbances, sliding mode control (SMC) has already been adopted as the mainstream solution. Leveraging the robustness of SMC in handling uncertainties and disturbances, Ref. [11] proposed a nonsingular terminal SMC to study the finite-time trajectory tracking problem for AUV. Based on a super-twisting algorithm, Ref. [12] designed a finite-time formation scheme for underactuated multi-AUVs with uncertainties. To

further actively compensate for lumped disturbances, the radial basis function neural network (RBFNN) is often integrated into the control framework. It can learn online and approximate unknown nonlinear dynamics, thereby significantly reducing reliance on prior knowledge such as the upper bounds of uncertainties [13]. The stability analyses for the closed-loop systems in the aforementioned studies typically only guarantee that the tracking error can asymptotically achieve a certain neighborhood of the equilibrium point [10–13]. However, some practical AUV tasks need to be completed within strictly specified timeframes while overcoming the aforementioned challenges.

To remove the reliance of convergence time upon initial conditions and achieve convergence performance determined solely by controller design parameters, fixed-time stability theory has been introduced into control system design [14,15]. The fixed-time control (FXTC) guarantees that the system state achieve a bounded of the equilibrium point within a fixed time, which is irrelevant to the initial conditions. In [16], a formation FXTC scheme was presented for multi-AUVs with additional disturbances and unmeasurable velocities to accomplish the trajectory tracking task. In [17], based on a dynamic event-triggered scheme, a FXTSMC strategy was proposed for AUV subject to additional disturbances and control input saturation. To eliminate potential singularities in classical terminal SMC while coping with the severe structural difficulties of underactuated AUVswhere the independent control inputs are fewer than the degrees of freedoma more robust fixed-time framework is urgently required. To overcome the coupled hydrodynamics and parameter variations without initial state dependency, a FXT nonsingular terminal SMC (FXTNTSMC) strategy based on adaptive RBFNN is proposed, which significantly accelerates the system's convergence rate and enhances tracking robustness.

While strictly guaranteeing the convergence time for high-precision trajectory tracking of underactuated AUVs, ensuring transient performance is also a concern that needs to be addressed. For this purpose, prescribed performance control (PPC) has been widely studied in [18]. Traditional PPC predefines a time-varying and convergent performance function as the error boundary. By employing error transformation techniques, it maps the constrained tracking error into an unconstrained variable, thereby theoretically ensuring that the transient and steady-state behavior of the error always remains within the envelope specified by the designer [19–21]. However, its preset performance boundary is rigid and fixed. When the system encounters large-magnitude disturbances, the tracking error may reach or exceed this rigid boundary, potentially causing the control input to increase sharply or even leading to system instability [22]. To overcome this defect, flexible PPC has been proposed. Specifically, it permits the performance envelope to be dynamically adjusted when necessary, proactively expanding the boundaries when the tracking error is on the verge of violating constraints to rule out controller singularities, and subsequently contracting them back to restore the nominal preset performance once the system stabilizes [23]. However, existing flexible PPC strategies are typically a passive response mechanism [24–26]. Their boundary adjustments are often executed only after the tracking error has critically approached or marginally breached the baseline thresholds, leaving the system highly vulnerable to transient instability. Consequently, such delayed corrections are frequently either obsolete or prone to inducing severe control chattering. To overcome these deficiencies, a predictive monitoring and adaptive tuning mechanism is highly essential. This mechanism dynamically relaxes the performance bounds upon detecting early signs of constraint violation, thereby eliminating singularities and safeguarding closed-loop stability. Once environmental threats subside, the envelopes automatically recover to their nominal states to preserve the desired tracking specifications. This strategically resolves the critical challenge of ensuring reliable and smooth transient/steady-state performance for the tracking errors of underactuated AUVs.

Inspired by study of the above literatures, this paper researches adaptive RBFNN-based FXTNTSMC issue for underactuated AUV with flexible PPC and uncertain dynamics. The primary contributions are listed as follows:

(i) Unlike existing flexible PPC schemes of [24–26] that passively adjust boundaries after error degradation, a proactive risk-monitoring mechanism based on a zeroing barrier function is devised. It actively predicts the constraint violation trend to relax boundaries in advance under large disturbances, eliminating controller singularities while ensuring reliable transient and steady-state performances.

(ii) Compared with the conventional finite-time sliding mode control (FTSMC) in [11], a novel FXTNTSMC strategy is designed. It structurally eliminates the singularity problem without requiring complex virtual control laws, and ensures the absolute convergence time is entirely independent of initial conditions, thereby achieving superior tracking accuracy.

(iii) In contrast to robust controllers relying heavily on high-gain discontinuous terms that induce severe chattering, an adaptive RBFNN is embedded to dynamically approximate the lumped disturbance online. This significantly reduces the required robust switching gain and fundamentally suppresses actuator chattering for practical AUV systems.

Notation 1. *$R^{a\times b}$ represents a set of $a \times b$ real matrices; R^n is n-dimensional Euclidean space. The X^{T} denotes transposition of matrix X. $X > 0$ represents the matrix X is a positive definite matrix. For $\boldsymbol{s} = [s_1, s_2, ..., s_n]^{\mathrm{T}}$,*

$\text{sig}^m(s) = [|s_1|^m \text{sign}(s_1), ..., |s_n|^m \text{sign}(s_n)]^{\text{T}}$. $\text{diag}\{...\}$ *is a diagonal matrix.*

2. Preliminary

2.1. System Introduction

Generally speaking, a AUV with six degrees-of-freedom (DOFs) as depicted in Figure 1, since AUVs typically adopt axially symmetric slender body structures (such as torpedo shapes), their roll motion around the x-axis, whether in terms of dynamic characteristics or its impact on overall translation and other steering motions, can be almost negligible. Therefore, ignoring the roll degree of freedom does not lose the generality of the problem, and can significantly reduce the complexity of the model and the difficulty of control design. An AUV mathematical model with five DOFs can be expressed as follows:

$$\begin{cases} \dot{\eta} = J(\eta)v, \\ M\dot{v} + C(v)v + D(v)v + G(\eta) = \tau + \omega, \end{cases} \tag{1}$$

where $\eta = [x, y, z, \theta, \varphi]^{\text{T}}$, $v = [u, v, w, q, r]^{\text{T}}$ represent the position vector and velocity vector of the AUV, respectively. $J(\eta)$ represents configuration-dependent transformation matrix. M is the symmetric matrix representing the inertia of system, $C(v) = C_0 + \Delta C$ means the Coriolis and centripetal matrix, $D(v) = D_0 + \Delta D$ means the hydrodynamic damping matrix, $G(\eta)$ represents the restoring forces vector, where M, C_0, and D_0 mean the normal value matrixs, ΔC, ΔD are the uncertain parameter matrix. $\tau = [\tau_u, 0, 0, \tau_q, \tau_r]^{\text{T}}$ represents control input vector of underactuated AUV; $\omega = [\omega_u, \omega_v, \omega_w, \omega_q, \omega_r]^{\text{T}}$ represents additional disturbances vector in the ocean environment. $J(\eta)$, M, C_0, D_0 and G are given as follows:

$$J(\eta) = \begin{bmatrix} J_1(\eta) & 0_{3\times2} \\ 0_{2\times3} & J_2(\eta) \end{bmatrix}, J_1(\eta) = \begin{bmatrix} \cos\theta\cos\varphi & -\sin\varphi & \sin\theta\cos\varphi \\ \cos\theta\sin\varphi & \cos\varphi & -\sin\varphi \\ -\sin\varphi & 0 & \cos\varphi \end{bmatrix}, J_2(\eta) = \begin{bmatrix} 1 & 0 \\ 0 & \frac{1}{\cos\theta} \end{bmatrix},$$

$$C_0 = \begin{bmatrix} 0 & 0 & 0 & m_{33}w & -m_{22}v \\ 0 & 0 & 0 & 0 & m_{11}u \\ 0 & 0 & 0 & -m_{11}u & 0 \\ -m_{33}w & 0 & m_{11}u & 0 & 0 \\ m_{22}v & -m_{11}u & 0 & 0 & 0 \end{bmatrix},$$

$$M = \text{diag}\{m_{11}, m_{22}, m_{33}, m_{44}, m_{55}\},$$

$$D_0 = \text{diag}\{d_{11}, d_{22}, d_{33}, d_{44}, d_{55}\},$$

$$G = [0, 0, 0, \rho g \nabla \overline{GM}_L \sin\theta, 0]^{\text{T}}.$$

So as to solve the underactuated control problem, we redefined position vector η_1 of AUVs as follows:

$$\eta_1 = \begin{bmatrix} x + \ell\cos\theta\cos\varphi \\ y + \ell\cos\theta\sin\varphi \\ z - \ell\sin\theta \end{bmatrix}, \tag{2}$$

where ℓ represents the distance from the action point of control force to the barycenter of AUVs as shown in Figure 1. Then, according to (1) and (2), we can get the following equations:

$$\dot{\eta}_1 = J_3 v_1 + J_4, \tag{3}$$

$$\bar{M}\dot{v}_1 + \bar{C}v_1 + \bar{D}v_1 + \bar{G} = \bar{\tau} + \bar{\omega}, \tag{4}$$

where $v_1 = [u, q, r]^{\text{T}}$, $\bar{\omega} = [\omega_u, \omega_q, \omega_r]^{\text{T}}$, $\bar{\tau} = [\tau_u, \tau_q, \tau_r]^{\text{T}}$ and $\bar{G}(\eta) = [0, \rho g \nabla \overline{GM}_L \sin\theta, 0]^{\text{T}}$, $J_3, J_4, \bar{M}, \bar{C}, \bar{D}$ represented as follows:

$$J_3 = \begin{bmatrix} \cos\theta\cos\varphi & -\ell\sin\theta\cos\varphi & -\ell\sin\varphi \\ \cos\theta\sin\varphi & -\ell\sin\theta\sin\varphi & \ell\cos\varphi \\ -\sin\theta & -\ell\cos\varphi & 0 \end{bmatrix}, J_4 = \begin{bmatrix} -v\sin\varphi + w\sin\theta\cos\varphi \\ v\cos\varphi + w\sin\theta\sin\varphi \\ w\cos\theta \end{bmatrix},$$

$$\bar{C} = \begin{bmatrix} 0 & m_{33}w & -m_{22}v \\ (m_{11}-m_{33})w & 0 & 0 \\ (m_{22}-m_{11})v & 0 & 0 \end{bmatrix},$$

$$\bar{M} = \mathrm{diag}\{m_{11}, m_{44}, m_{55}\}, \bar{D} = \mathrm{diag}\{d_{11}, d_{44}, d_{55}\}.$$

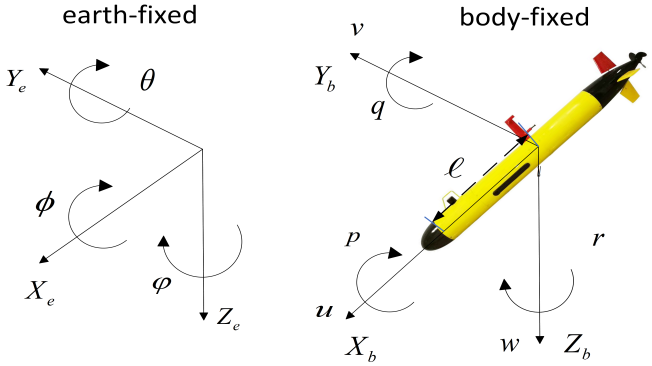

Figure 1. Reference frame of AUVs.

The research control objective is to design a FXTNTSMC strategy based on adaptive RBFNN and flexible prescribed performance for underactuated AUV subject to uncertain dynamics and additional disturbances, ensuring precise tracking of a reference trajectory η_d within a fixed time and the position error converges to a bounded region within the prescribed performance constraints. And let reference trajectory $\eta_d = [\eta_{d1}, \eta_{d2}, \eta_{d3}]^{\mathrm{T}}$. In additional, to meet the needs of the subsequent proofs, some important lemmas and assumptions are formulated:

Assumption 1 ([13]). *The uncertain dynamics and additional disturbances of underactuated AUVs are bounded and time-varying.*

Assumption 2 ([3]). *During the trajectory tracking process, the pitch angle θ and roll angle φ of the AUV are constrained within $(-\frac{\pi}{2}, \frac{\pi}{2})$.*

Lemma 1 ([27]). *For the following system: $\dot{x} = f(t)$, $x(0) = x_0$, if there are Lyapunov function $V(x)$ and parameters $m_1 > 0$, $m_2 > 0$, $0 < n_1 < 1$, $n_2 > 1$, $0 < m_3 < \infty$ satisfying:*

$$\dot{V}(x) \leq -m_1 V^{m_2}(x) - n_1 V^{n_2}(x) + m_3, \tag{5}$$

then the system is able to achieve practical fixed-time stable. The fixed time and the convergence bounded can been obtained

$$T \leq \frac{1}{m_1\gamma_1(1-m_2)} + \frac{1}{n_1\gamma_1(1-n_2)}, \tag{6}$$

$$\Lambda = \left\{ x \middle| V \leq \min\left\{ \left[\frac{m_3}{m_1(1-\gamma_1)}\right]^{\frac{1}{m_2}}, \left[\frac{m_3}{n_1(1-\gamma_1)}\right]^{\frac{1}{m_4}} \right\} \right\}, \tag{7}$$

where $0 < \gamma_1 < 1$.

Lemma 2 ([28]). *(Young's Inequality) For constants $\rho, \vartheta \in \mathrm{R}$, there exist the following inequation:*

$$\rho\vartheta \leq \frac{m_5^{m_4}}{m_4}|\rho|^{m_4} + \frac{1}{m_6 m_5^{m_6}}|\vartheta|^{m_6}, \tag{8}$$

where $m_4 > 1$, $m_5 > 0$, $m_6 > 1$ and $(m_4 - 1)(m_6 - 1) = 1$.

Lemma 3 ([29]). *For a vector $x_j \in \mathrm{R}^n$, constants $0 < m_7 \leq 1, m_8 > 1$, there exist the following inequations :*

$$\left(\sum_{j=1}^{n}|x_j|\right)^{m_7} \leq \sum_{j=1}^{n}|x_j|^{m_7}, \tag{9}$$

$$\left(\sum_{j=1}^{n}|x_j|\right)^{m_8} \leq n^{m_8-1}\sum_{j=1}^{n}|x_j|^{m_8}. \tag{10}$$

Lemma 4 ([30]). *For a smooth function $\xi_1(t)$, if the following two conditions hold: $\dot{\xi}_1(t)+\delta\xi_1(t)\geqslant 0$ and $\xi_1(0)\geqslant 0$, $\delta>0$ is a constant, then $\xi_1(t)>0$ for all $t>0$.*

2.2. RBFNN

The RBFNN is extensive utilized to approximate nonlinear continuous functions based on its fast convergence and simple structure. Its basic framework is composed of input, hidden and output layers, where Gaussian function is used as radial basis function to deactivate neurons in the hidden layer. The RBFNN approximation function as follows:

$$\bar{\hbar}(x)=\bar{W}^{\mathrm{T}}\psi(x), \tag{11}$$

where $\bar{W}\in \mathrm{R}^{m\times n}$ means the weight matrix, x is the input vector, $\psi(x)$ means Gaussian function,

$$\psi_i(x)=\exp(-\tfrac{\|x-c_i\|^2}{2b_i^2}), \tag{12}$$

where $i=1,2,...,m$, b_i means the width of $\psi(x)$, c_i means the center vector, m is the number of nodes in the hidden layer. Then, by utilizing RBFNN to approximate function $\hbar(x)$ as follows

$$\hbar(x)=\hat{W}^{\mathrm{T}}\psi(x)+\varsigma(x) \tag{13}$$

where $\hat{W}$ represents the ideal weight matrix, $\varsigma(x)$ represents the error between $\bar{\hbar}(x)$ and $\hbar(x)$, $\varsigma(x)\leq\varsigma_1,\varsigma_1>0$.

3. Main Results

In this section, a FXTNTSMC strategy is designed to finish the trajectory tracking task based on adaptive RBFNN and FPPC. The block diagram of adaptive FXTNTSMC strategy process is shown in Figure 2.

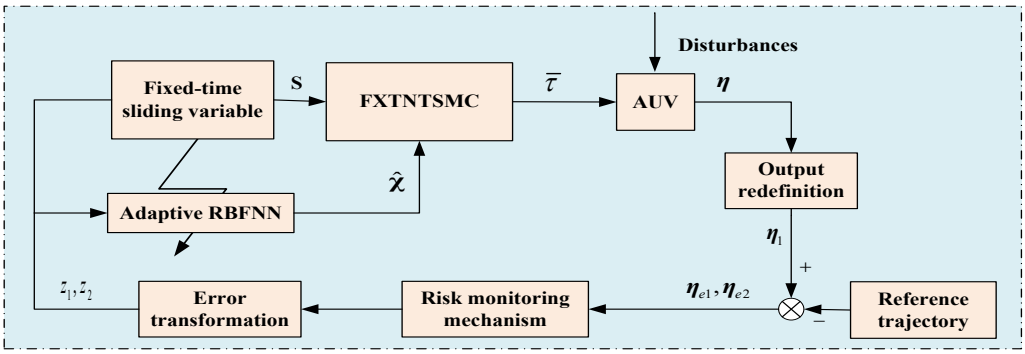

Figure 2. Block diagram of adaptive FXTNTSMC strategy.

3.1. Error Transformation

Let the tracking errors $\eta_{e1}=\eta_1-\eta_d$, $\dot{\eta}_{e1}=\eta_{e2}$, then according to Equations (2)–(4), we can obtain the following equations:

$$\dot{\eta}_{e1}=J_3v_1+J_4-\dot{\eta}_d, \tag{14}$$

$$\dot{\eta}_{e2}=\dot{J}_3v_1+\dot{J}_4+J_3\bar{M}^{-1}(-\bar{C}_0v_1-\bar{D}_0v_1-\bar{G}+\bar{\tau})+\chi-\ddot{\eta}_d, \tag{15}$$

in which $\chi=J_3\bar{M}^{-1}(\bar{\omega}-\Delta\bar{C}v_1-\Delta\bar{D}v_1)$ is unknown lumped disturbance. At the same time, it is necessary to ensure that the tracking error remain within the prescribed performance limits, that is

$$-\rho_i(t)<\eta_{e1,i}(t)<\rho_i(t), \tag{16}$$

with $i=1,2,3$, $\rho_i(t)$ is the prescribed performance function. Next, define an error transformation function as

$$z_{1,i} = \frac{1}{2}\ln\left(\frac{\frac{\eta_{e1,i}(t)}{\rho_i(t)}+1}{1-\frac{\eta_{e1,i}(t)}{\rho_i(t)}}\right). \tag{17}$$

This transformation ensures that the system states before and after the transformation exhibit the same monotonicity; therefore, based on this transformation, as long as the transformed system is stable, it is guaranteed that the original system also satisfies the performance requirements. Based on the above equation, the constraints mentioned above can be expressed as $-\infty < z_{1,i} < +\infty$. And its time derivative can be expressed as

$$\dot{z}_{1,i} = \Omega_i \dot{\eta}_{e1,i} - \mho_i \eta_{e1,i}, \tag{18}$$

where $\Omega_i = \frac{\rho_i(t)}{\rho_i^2(t)-\eta_{e1,i}^2(t)}$, $\mho_i = \frac{\dot{\rho}_i(t)}{\rho_i^2(t)-\eta_{e1,i}^2(t)}$. Let $z_1 = [z_{1,i}, z_{2,i}, z_{3,i}]^{\mathrm{T}}$, $\Omega = \mathrm{diag}\{\Omega_1, \Omega_2, \Omega_3\}$, $\mho = \mathrm{diag}\{\mho_1, \mho_2, \mho_3\}$, we can obtain that

$$\dot{z}_1 = \Omega \dot{\eta}_{e1} - \mho \eta_{e1}. \tag{19}$$

3.2. PPC Based on Risk Monitoring Mechanism

In this section, a constraint monitoring mechanism is proposed to assess whether the state error of the underactuated AUV shows a tendency to violate the prescribed performance constraints. The mechanism provides a basis for deciding subsequent adjustments of the prescribed performance function.

Based on Lemma 4, a zeroing barrier function $\zeta_{1,i}(t)$ is constructed for the state error of the underactuated AUV:

$$\zeta_{1,i}(t) = 1 - \mathfrak{k}_i^{\,2} \tag{20}$$

with $\mathfrak{k}_i = \eta_{e1,i}(t)/\rho_i(t)$. When $\zeta_{1,i}(t) > 0$, it corresponds exactly to the safe region where the prescribed performance constraints are satisfied. However, monitoring only the current sign of $\zeta_{1,i}(t)$ is insufficient. When it approaches zero, the system is already on the verge of danger and may not have enough time to respond. Therefore, an indicator capable of predicting the future trend is needed:

$$\hbar_{1,i}(t) = \dot{\zeta}_{1,i}(t) + \delta\zeta_{1,i}(t). \tag{21}$$

Based on Lemma 4 and Equation (21), the safety conditions can be directly evaluated as follows:

(i) When $\hbar_{1,i}(t) \geq 0$ and $\zeta_{1,i}(t) > 0$, it indicates that the error state of the underactuated AUV system is safe and there is no risk of violating the constraints.

(ii) When $\hbar_{1,i}(t) < 0$ and $\zeta_{1,i}(t) > 0$, it means that the error state of the underactuated AUV system currently satisfies the constraints but is at risk of approaching the constraint boundary.

(iii) When $\hbar_{1,i}(t) > 0$ and $\zeta_{1,i}(t) < 0$, it implies that the error state of the underactuated AUV system has already violated the constraints but shows a trend towards satisfying the constraints.

A smooth indicator function $\gamma(\hbar_{1,i})$ is further designed as:

$$\gamma(\hbar_{1,i}) = \begin{cases} 1, & \hbar_{1,i} \leq 0 \\ 1 - 3\left(\dfrac{\hbar_{1,i}}{2\varepsilon}\right)^2 + 2\left(\dfrac{\hbar_{1,i}}{2\varepsilon}\right)^3, & 0 < \hbar_{1,i} < 2\varepsilon \\ 0, & \hbar_{1,i} \geq 2\varepsilon \end{cases} \tag{22}$$

where $\varepsilon > 0$ is a small constant. Then, we can obtain that

(i) When $\hbar_{1,i}(t) \leq 0$, it indicates that the error state of the underactuated AUV is at high risk of violating the constraints, requiring immediate intervention.

(ii) When $0 < \hbar_{1,i} < 2\varepsilon$, this phase represents a smooth transition.

(iii) When $\hbar_{1,i}(t) \geq 2\varepsilon$, the output is 0, signifying that the error state of the underactuated AUV either satisfies the constraints or shows a trend towards satisfying them, thus requiring no additional intervention.

To address the potential risk of constraint violation by the error state in underactuated AUVs, a flexible prescribed performance constraint is developed by introducing an additional adjustment term $\bar{\rho}_i(t)$. The prescribed

performance function is designed as follows:

$$\rho_i(t) = \rho_{1i}(t) + \bar{\rho}_i(t) \tag{23}$$

where $\rho_{1i}(t)$ is the baseline performance envelope and $\bar{\rho}_i(t)$ denotes the dynamic adjustment term, which are given by:

$$\rho_{1i}(t) = \begin{cases} (\rho_{i,0} - \rho_{i,\infty})\, e^{\left(1 - \frac{T}{T-t}\right)}, & 0 \le t < T, \\ \rho_{i,\infty}, & T \le t, \end{cases} \tag{24}$$

$$\dot{\bar{\rho}}_i(t) = -\lambda_1 \bar{\rho}_i(t) + \lambda_2 \gamma(\hbar_i) \tanh\left(\frac{|\mathfrak{k}_i|}{\lambda_3}\right), \tag{25}$$

with $\rho_{i,0}$ being the initial value of the nominal envelope, $\rho_{i,\infty}$ being the steady-state value of the nominal envelope, T being the prescribed time window during which the nominal envelope decays from $\rho_{i,0}$ to $\rho_{i,\infty}$, λ_1, λ_2 and λ_3 being given positive constants.

Remark 1. *The flexible performance boundary $\rho_i(t) = \rho_{1i}(t) + \bar{\rho}_i(t)$ is strictly positive and bounded. The nominal function $\rho_{1i}(t) > 0$ strictly holds by definition. The dynamic adjustment term $\bar{\rho}_i(t)$ is driven by Equation (25). Since $\lambda_1, \lambda_2 > 0$ and the indicator function $\gamma(\hbar_i) \ge 0$, the input to the first-order filter is always non-negative. Due to the initial condition $\bar{\rho}_i(0) = 0$, it follows that $\bar{\rho}_i(t) \ge 0$ for all $t \ge 0$. Consequently, $\rho_i(t) \ge \rho_{1i}(t) > 0$. Furthermore, when $\mathfrak{k}_i$ approaches the critical boundary ± 1, the term $\lambda_2 \gamma(\hbar_i) \tanh(|\mathfrak{k}_i|/\lambda_3)$ dynamically injects a positive growth rate into $\bar{\rho}_i(t)$, actively expanding the boundary $\rho_i(t)$. This proactive expansion strictly prevents $|\mathfrak{k}_i|$ from reaching 1, thereby naturally avoiding the singularity of the controller.*

3.3. Adaptive RBFNN-Based FXTNTSMC

In this section, an improved FXTNTSMC is proposed to make the state error converge based on adaptive RBFNN, which is showed:

$$S = \dot{z}_1 + S_1, \tag{26}$$

where $S_1 = [S_{11}, S_{12}, S_{13}]^{\mathrm{T}}$ is used to avoid the singularity of FXTNTSMC, and S_{1i} is given below

$$S_{1i} = \begin{cases} \mathrm{sig}^{\alpha}(S_{ei}) & if|S_{ei}| > \sigma \\ \beta_1 S_{ei} + \beta_2 \mathrm{sign}(S_{ei}) S_{ei}^2 & if|S_{ei}| \le \sigma \end{cases}, \tag{27}$$

$$S_{ei} = a_1 \mathrm{sig}^{a_2}(z_{1,i}) + a_3 \mathrm{sig}^{a_4}(z_{1,i}), \tag{28}$$

where $\beta_1 = (2-\alpha)\sigma^{\alpha-1}$, $\beta_2 = (\alpha-1)\sigma^{\alpha-2}$, $a_1 > 0$, $b_1 > 0$, $0.5 \le a_2 < 1$, $b_2 > 1$, $\alpha > 0.5$, $a_2\alpha < 1$, $b_2\alpha > 1$, $\sigma > 0$ are the relevant control parameters.

According to Equations (19),(26)–(28), the derivative of sliding variable S can be obtained:

$$\begin{aligned} \dot{S} =& \ddot{z}_1 + \dot{S}_1 \\ =& \Omega(\dot{J}_3 v_1 + \dot{J}_4 + J_3 \bar{M}^{-1}(-\bar{C}_0 v_1 - \bar{D}_0 v_1 - \bar{G} + \bar{\tau}) + \chi - \ddot{\eta}_d) \\ &+ \dot{\Omega}\dot{\eta}_{ei} - \dot{\mho}\eta_{ei} - \mho\dot{\eta}_{ei} + \dot{S}_1. \end{aligned} \tag{29}$$

Then, the control law of adaptive RBFNN-based FXTNTSMC can be designed by (25)-(28):

$$\bar{\tau} = \bar{\tau}_{eq} + \bar{\tau}_{sm}, \tag{30}$$

$$\bar{\tau}_{eq} = \bar{M} J_3^{-1}[\Omega^{-1}(\dot{\mho}\eta_{ei} + \mho\dot{\eta}_{ei} - \dot{\Omega}\dot{\eta}_{ei} - \dot{S}_1) - \dot{J}_3 v_1 - \dot{J}_4 - \bar{\chi} + \ddot{\eta}_d] + \bar{C}_0 v_1 + \bar{D}_0 v_1 + \bar{G}, \tag{31}$$

$$\bar{\tau}_{sm} = \bar{M} J_3^{-1}(-\kappa_1 \mathrm{sign}(S) - \kappa_2 \mathrm{sig}^3(S) - \kappa_3 S), \tag{32}$$

where $\kappa_1 > 0$, $\kappa_2 > 0$, $\kappa_3 > 0.5$. $\bar{\tau}_{sm}$ is the robust controller, $\bar{\tau}_{eq}$ is the equivalent controller, and the estimated value $\bar{\chi}$ can be obtained by applying RBFNN to approximate the nonlinear term χ as follows:

$$\bar{\chi} = \bar{W}^{\mathrm{T}} \psi(x), \tag{33}$$

where $\bar{W} = \mathrm{diag}\{\bar{W}_1, \bar{W}_2, \bar{W}_3\}$ is the estimation of $\hat{W}$, $x = [\eta_{e1}^{\mathrm{T}}, \eta_{e2}^{\mathrm{T}}]^{\mathrm{T}}$ means the input of the approximation

function. Besides, the adaptive law of $\bar{W}_i$ is given

$$\dot{\bar{W}}_i = \psi_i(x)S_i - \bar{W}_i\bar{W}_i^{\mathrm{T}}\bar{W}_i. \tag{34}$$

Remark 2. *It is worth noting that while traditional SMC relies heavily on a high-gain discontinuous sign function to suppress unknown disturbances, which often inducing severe chattering. The proposed control scheme significantly mitigates this issue by utilizing an adaptive RBFNN to dynamically approximate the lumped disturbance χ online. Because the adaptive RBFNN accurately compensates for the majority of the continuous disturbances, the robust switching gain κ_1 associated with the sign(S) function only needs to be sufficiently large to cover the RBFNN's small approximation error $\varsigma(x)$, rather than the entire disturbance magnitude. Consequently, the amplitude of the discontinuous term is heavily reduced, effectively suppressing chattering at its source and ensuring smooth simulation results.*

3.4. Stability Analysis of System

Theorem 1. *Considering the underactuated AUV system (1) with uncertain dynamics and additional disturbances under Assumption 1. By the FXTNTSMC laws (30)–(32) and the weight adaptive law (34), if there exist parameters satisfying $\kappa_1 > 0$, $\kappa_2 > 0$, $\kappa_3 > 0.5$, $a_1 > 0$, $b_1 > 0$, $0.5 \le a_2 < 1$, $b_2 > 1$, $\alpha > 0.5$, $a_2\alpha < 1$, $b_2\alpha > 1$, $\sigma > 0$, ς_1, $\lambda_1 > 0$ and $\lambda_2 > 0$, then the trajectory tracking error is able to converge to a finite region within a fixed time $T = T_1 + T_2$.*

Proof. First, we demonstrate that the sliding variable S can reach a finite region Λ at a fixed time T_1. The Lyapunov function is designed:

$$V = \frac{1}{2}S^{\mathrm{T}}S + \frac{1}{2}\sum_{i=1}^{3}\tilde{W}_i^{\mathrm{T}}\tilde{W}_i. \tag{35}$$

Calculating the time derivative of $V(t)$ yields:

$$\begin{aligned}
\dot{V} =& S^{\mathrm{T}}\dot{S} + \sum_{i=1}^{3}\tilde{W}_i^{\mathrm{T}}\dot{\tilde{W}}_i \\
=& S^{\mathrm{T}}(-\kappa_1\mathrm{sign}(S) + \kappa_2\mathrm{sig}^3(S) - \kappa_3 S - \tilde{W}^{\mathrm{T}}\psi(x) + \varsigma(x)) + \sum_{i=1}^{3}\tilde{W}_i^{\mathrm{T}}(\psi_i(x)S_i - \bar{W}_i\bar{W}_i^{\mathrm{T}}\bar{W}_i) \\
=& S^{\mathrm{T}}\varsigma(x) - \sum_{i=1}^{3}(\kappa_1|S_i| + \kappa_2|S_i|^4 + \kappa_3 S_i^2 + \tilde{W}_i^{\mathrm{T}}\bar{W}_i\bar{W}_i^{\mathrm{T}}\bar{W}_i),
\end{aligned} \tag{36}$$

where $\tilde{W} = \bar{W}_i - \hat{W}_i$. Based on Young's inequality, $S^{\mathrm{T}}\varsigma(x)$ can be express as:

$$S^{\mathrm{T}}\varsigma(x) \le \frac{1}{2}S^{\mathrm{T}}S + \frac{1}{2}\varsigma_1^2. \tag{37}$$

Then, substituting (37) into (36) results in:

$$\begin{aligned}
\dot{V} \le& \frac{1}{2}\varsigma_1^2 - \sum_{i=1}^{3}(\kappa_1|S_i| + \kappa_2|S_i|^4 + (\kappa_3 - \frac{1}{2})S_i^2 + \left\|\tilde{W}_i\right\|^4 + \|\bar{W}_i\|^2(\left\|\tilde{W}_i\right\|^2 + \tilde{W}_i^{\mathrm{T}}\bar{W}_i) \\
&+ 3\left\|\tilde{W}_i\right\|^2\tilde{W}_i^{\mathrm{T}}\bar{W}_i + 2\left\|\tilde{W}_i^{\mathrm{T}}\bar{W}_i\right\|^2),
\end{aligned} \tag{38}$$

Applying Lemma 3, we can get the following inequations:

$$-\left\|\tilde{W}_i\right\|^2\tilde{W}_i^{\mathrm{T}}\bar{W}_i \le \left\|\tilde{W}_i\right\|^3\|\bar{W}_i\| \le \frac{3}{4}\lambda_1^{\frac{4}{3}}(\left\|\tilde{W}_i\right\|^3)^{\frac{4}{3}} + \frac{1}{4\lambda_1^4}\|\bar{W}_i\|^4, \tag{39}$$

$$-\|\bar{W}_i\|^2\tilde{W}_i^{\mathrm{T}}\bar{W}_i \le \|\bar{W}_i\|^3\left\|\tilde{W}_i\right\| \le \frac{3}{4}\lambda_2^{\frac{4}{3}}(\|\bar{W}_i\|^3)^{\frac{4}{3}} + \frac{1}{4\lambda_2^4}\left\|\tilde{W}_i\right\|^4, \tag{40}$$

$$-\left\|\tilde{W}_i^{\mathrm{T}}\bar{W}_i\right\|^2 \le -\left\|\tilde{W}_i\right\|^2\|\bar{W}_i\|^2 \le -\|\bar{W}_i\|^2(2\left\|\tilde{W}_i\right\| - 1). \tag{41}$$

Recalling $\kappa_3 - \frac{1}{2} > 0$, $2\left\|\tilde{W}_i^{\mathrm{T}}\bar{W}_i\right\|^2 \ge 0$, we can obtain that:

$$\begin{aligned}\dot{V} \leq & \frac{1}{2}\varsigma_1^2 - \sum_{i=1}^{3}(\kappa_1|S_i| + \kappa_2|S_i|^4 + 2\left\|\bar{W}_i\right\|^2\left\|\tilde{W}_i\right\| + (1 - \frac{9}{4}\lambda_1^{\frac{4}{3}} - \frac{1}{4\lambda_2^4})\left\|\tilde{W}_i\right\|^4 + \left\|\bar{W}_i\right\|^2 \\ & + (\frac{3}{4}\lambda_2^{\frac{4}{3}} + \frac{3}{4\lambda_1^4})\left\|\bar{W}_i\right\|^4) \\ \leq & -\zeta_1 V^{\frac{1}{2}} - \zeta_2 V^2 + \zeta_3,\end{aligned} \tag{42}$$

where $\zeta_1 = \min\{\sqrt{2}\kappa_1, 2\sqrt{2}\left\|\bar{W}_i\right\|^2\}$, $\zeta_2 = \min\{4\kappa_2, 4-9\lambda_1^{\frac{4}{3}} - \frac{1}{\lambda_2^4}\}$, $\zeta_3 = \frac{1}{2}\varsigma_1^2 + \sum_{i=1}^{3}(\left\|\bar{W}_i\right\|^2 + (\frac{3}{4}\lambda_2^{\frac{4}{3}} + \frac{3}{4\lambda_1^4})\left\|\bar{W}_i\right\|^4)$. According to Lemma 1, the designed sliding variable S are able to converge to a finite region Λ within a fixed time T_1.

$$T_1 \leq T_{\max} = \frac{2}{\zeta_1\gamma_1} + \frac{1}{\zeta_2\gamma_1}, \tag{43}$$

$$\Lambda = \left\{\vartheta \middle| V(\vartheta) \leq \min\left\{\left[\frac{\zeta_3}{\zeta_1(1-\gamma_1)}\right]^2, \left[\frac{\zeta_3}{\zeta_2(1-\gamma_1)}\right]^{\frac{1}{2}}\right\}\right\}, \tag{44}$$

where $\vartheta = [S^{\mathrm{T}}, \tilde{W}_1^{\mathrm{T}}, \tilde{W}_2^{\mathrm{T}}, \tilde{W}_2^{\mathrm{T}}]^{\mathrm{T}}$, $0 < \gamma_1 < 1$.

Next, demonstrating trajectory tracking errors $z_{1,i}$ can achieve a bounded region within a fixed time T_2. Firstly, if $z_{1,i} > 0$, we can obtain that $S_{ei} = a_1\mathrm{sig}^{a_2}(z_{1,i}) + a_3\mathrm{sig}^{a_4}(z_{1,i}) > 0$. Then, when $S_{ei} > \sigma$, according to Equations (26)–(28), the equation can be obtained:

$$\dot{z}_{1,i} = -(a_1 z_{1,i}^{a_2} + a_3 z_{1,i}^{a_4})^{\alpha} + S. \tag{44}$$

According to the above proof, the sliding variable S converges to a bounded region Λ within a fixed time T_1, meaning there exists a known small constant $\mathfrak{p} > 0$ such that $|S_i| \leq \mathfrak{p}$ holds. To address this residual perturbation, a tuning parameter $\mathfrak{g}_1 \in (0, 1)$ is introduced, allowing (44) to be bounded by the following inequality:

$$\dot{z}_{1,i} \leqslant -\mathfrak{g}_1(a_1 z_{1,i}^{a_2} + a_3 z_{1,i}^{a_4})^{\alpha} - (1-\mathfrak{g}_1)(a_1 z_{1,i}^{a_2} + a_3 z_{1,i}^{a_4})^{\alpha} + \mathfrak{p}. \tag{45}$$

Define the practical convergence residual neighborhood boundary of the state error $z_{1,i}$ as μ_1, satisfying $(1-\mathfrak{g}_1)(a_1\mu_1^{a_2} + a_3\mu_1^{a_4})^{\alpha} = \mathfrak{p}$. When $z_{1,i} > \mu_1$, the dominant control term overcomes the perturbation, and the differential inequality can be simplified as:

$$\dot{z}_{1,i} \leqslant -\mathfrak{g}_1(a_1 z_{1,i}^{a_2} + a_3 z_{1,i}^{a_4})^{\alpha}. \tag{46}$$

To determine the upper bound of the convergence time, let $\xi_{1i} = z_{1,i}^{1-a_2\alpha}$, we can obtain

$$\dot{\xi}_{1i} = -\mathfrak{g}_1(1-a_2\alpha)(a_1 + a_3\xi_1^{\lambda})^{\alpha} \tag{47}$$

where $\lambda = (a_4 - a_2)/(1 - a_2\alpha)$, then by calculating, the convergence time T_{21i} is able to be get as follows:

$$\begin{aligned}T_{21i} = & \lim_{\xi_{1i0}\to\infty}\frac{1}{\mathfrak{g}_1(1-a_2\alpha)}\int_{\mu_1^{1-a_2\alpha}}^{\xi_{1i0}}\frac{1}{(a_1+a_3\xi_1^{\lambda})^{\alpha}}d\xi_{1i} \\ = & \frac{1}{\mathfrak{g}_1(1-a_2\alpha)}(\int_1^{\infty}\frac{d\xi_{1i}}{(a_1+a_3\xi_1^{\lambda})^{\alpha}} + \int_{\mu_1^{1-a_2\alpha}}^{1}\frac{d\xi_{1i}}{(a_1+a_3\xi_1^{\lambda})^{\alpha}}) \\ \leqslant & \frac{1}{\mathfrak{g}_1(1-a_2\alpha)}(\int_1^{\infty}\frac{d\xi_{1i}}{a_3^{\alpha}\xi_1^{\lambda\alpha}} + \int_{\mu_1^{1-a_2\alpha}}^{1}\frac{d\xi_{1i}}{a_1^{\alpha}}) \\ \leqslant & \frac{1}{\mathfrak{g}_1(1-a_2\alpha)}(\frac{1}{a_3^{\alpha}(\lambda\alpha-1)} + \frac{1}{a_1^{\alpha}}) \\ = & \frac{1}{\mathfrak{g}_1}(\frac{1}{a_1^{\alpha}(1-a_2\alpha)} + \frac{1}{a_3^{\alpha}(a_4\alpha-1)}).\end{aligned} \tag{48}$$

when $0 < S_{ei} < \sigma$, according to Equations (26)–(28), we can obtain:

$$\dot{z}_{1,i} = -\beta_1(a_1 z_{1,i}^{a_2} + a_3 z_{1,i}^{a_4}) - \beta_2(a_1 z_{1,i}^{a_2} + a_3 z_{1,i}^{a_4})^2 + S. \tag{49}$$

Similarly, introducing a second tuning parameter $\theta_2 \in (0, 1)$ and defining the practical convergence boundary

μ_2 for this phase such that $(1-\theta_2)[\beta_1(a_1\mu_2^{a_2}+a_3\mu_2^{a_4})+\beta_2(a_1\mu_2^{a_2}+a_3\mu_2^{a_4})^2]=\mathfrak{p}$. When $z_{1,i}>\mu_2$, the equation can be bounded by:

$$\dot{z}_{1,i}\leqslant -\mathfrak{g}_2[\beta_1(a_1z_{1,i}^{a_2}+a_3z_{1,i}^{a_4})+\beta_2(a_1z_{1,i}^{a_2}+a_3z_{1,i}^{a_4})^2]. \tag{50}$$

Let $\xi_{2i}=z_{1,i}^{1-a_2}$, $\dot{\xi}_{2i}$ can be obtained:

$$\begin{aligned}\dot{\xi}_{2i}=&-\mathfrak{g}_2(1-a_2)(\beta_1(a_1+a_3z_{1,i}^{a_4-a_2})+\beta_2z_{1,i}^{-a_2}(a_1z_{1,i}^{a_2}+a_3z_{1,i}^{a_4})^2)\\ \leqslant&-\mathfrak{g}_2(1-a_2)\beta_1(a_1+a_3\xi_{2i}^{\lambda_1}),\end{aligned} \tag{51}$$

where $\lambda_1=(a_4-a_2)/(1-a_2)$, then T_{22i} is able to be calculated as:

$$\begin{aligned}T_{22i}\leq&\lim_{\xi_{2i0}\to\infty}\frac{1}{\mathfrak{g}_2(1-a_2)}\int_{\mu_2^{1-a_2}}^{\xi_{2i0}}\frac{1}{\beta_1(a_1+a_3\xi_{2i}^{\lambda_1})}d\eta_{e1i}\\ =&\frac{1}{\mathfrak{g}_2(1-a_2)}(\int_1^{\infty}\frac{d\xi_{2i}}{\beta_1(a_1+a_3\xi_{2i}^{\lambda_1})}+\int_{\mu_2^{1-a_2}}^{1}\frac{d\xi_{2i}}{\beta_1(a_1+a_3\xi_{2i}^{\lambda_1})})\\ =&\frac{1}{\mathfrak{g}_2\beta_1}(\frac{1}{a_1(1-a_2)}+\frac{1}{a_3(a_4-1)}).\end{aligned} \tag{52}$$

If $z_{1,i}<0$, the proof processes are similar with the case of $z_{1,i}>0$. When $S_{ei}<-\sigma$, T_{23i} is able to be calculated as:

$$T_{23i}=T_{21i}\leqslant\frac{1}{\mathfrak{g}_1}[\frac{1}{a_1^{\alpha}(1-a_2\alpha)}+\frac{1}{a_3^{\alpha}(a_4\alpha-1)}]. \tag{53}$$

when $0>S_{ei}>-\sigma$,

$$T_{24i}=T_{22i}\leqslant\frac{1}{\mathfrak{g}_2\beta_1}[\frac{1}{a_1(1-a_2)}+\frac{1}{a_3(a_4-1)}]. \tag{54}$$

In summary, the convergence time $T_2=\max\{T_{21i},T_{22i},T_{23i},T_{24i}\}$. The trajectory tracking error z_1 is able to converge to a small neighborhood of zero for $t\geq T_2$. This means that the underactuated AUV can track the reference trajectory η_d. □

4. Demonstrative Example

A series of numerical simulations are conducted to validate the effectiveness of the proposed FXTNTSMC strategy for the underactuated AUV system in this section. The motion model parameters of [5] is adopted to the simulation. The initial position and velocity are$\eta=[0,0.5,0,0,0]^{\mathrm{T}}$, $v=[0,0,0,0,0]^{\mathrm{T}}$. The uncertain parameters are $\Delta C=10\%C_0$ and $\Delta D=10\%D_0$. The ocean environmental disturbances are $\omega=[3\sin(0.2\pi t)_{\mathrm{N}},\sin(0.2\pi t)_{\mathrm{N}},\cos(0.1\pi t)_{\mathrm{N}},\cos(0.2\pi t)_{\mathrm{N}}\cdot\mathrm{m},\sin(0.1\pi t)+\cos(0.1\pi t)_{\mathrm{N}}\cdot\mathrm{m}]^{\mathrm{T}}$. The reference trajectory is $\eta_d=[4\cos(0.1t),4\sin(0.1t),-0.1t]^{\mathrm{T}}$.

The risk monitoring gain is set as $\delta=2$. The small constant defining the transition region in $\gamma(\chi_{1,i})$ is chosen as $\varepsilon=0.1$. The parameters for the baseline performance function $\rho_{1i}(t)$ are: initial value $\rho_{1,0}=5$, $\rho_{2,0}=0.5$, $\rho_{3,0}=0.2$, steady-state value $\rho_{i,\infty}=0.005$, and the prescribed convergence time $T=15$ s, for $i=1,2,3$. The parameters for the adjustment dynamics are set as: $\lambda_1=0.5$, $\lambda_2=0.3$, and $\lambda_3=0.1$. The number of hidden neurons in the RBFNN is $m=7$. The initial weights of the RBFNN are randomly initialized in the range $[0,1]$. The width of the Gaussian functions is $b_i=1.0$ for $i=1,\ldots,m$. The center vectors $\boldsymbol{c}_i$ of the Gaussian functions are randomly initialized in the range $[-1,1]$. The related control parameters are $\kappa_1=0.005$, $\kappa_2=0.8$, $\kappa_3=0.6$, $a_1=b_1=a_2=0.8$, $b_2=2$, $\alpha=0.6$, $\sigma=0.005$ and $\zeta_1=0.05$.

Figure 3 demonstrates that the trajectory of the underactuated AUV is able to converge to η_d under the FXTNTSMC strategy. Compared to FTSMC strategy of [11], this approach not only exhibits a faster convergence rate but also superior tracking performance, particularly in the X-axis direction visible from Figure 4. Figure 4 displays the trajectory tracking position comparison of each underactuated AUV in the X, Y, and Z directions. Figure 5 presents the tracking velocity curves of each underactuated AUV over time. The velocity chatter is also reduced when using the proposed control strategy. The comparison of control inputs presented in Figure 6 means that the FXTNTSMC strategy generates less chatter and offers better control effects. Figure 7 presents the tracking position error curves of each underactuated AUV over time, all remaining within the designed prescribed performance boundaries. Figure 8 shows the approximation error of the lumped disturbance χ, which can converge to zero over time. In summary, the proposed control strategy enables the underactuated AUV to accomplish trajectory tracking tasks under uncertainties dynamics and flexible prescribed performance, thereby enhancing energy utilization efficiency.

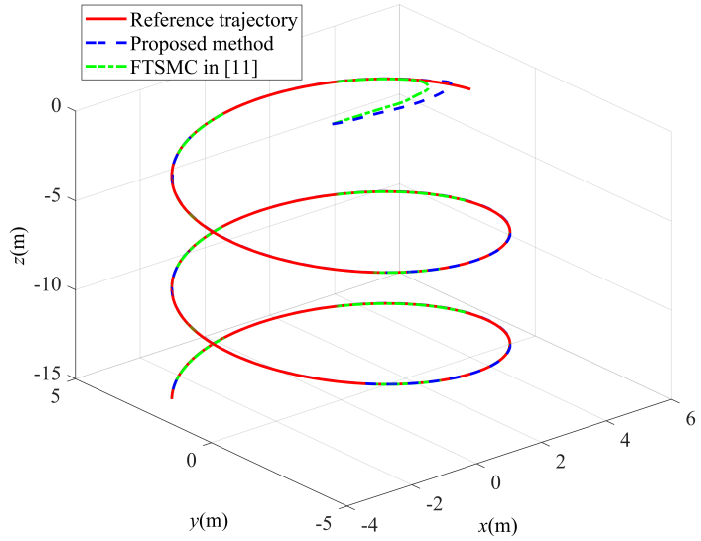

Figure 3. Trajectory tracking comparison of the underactuated AUV.

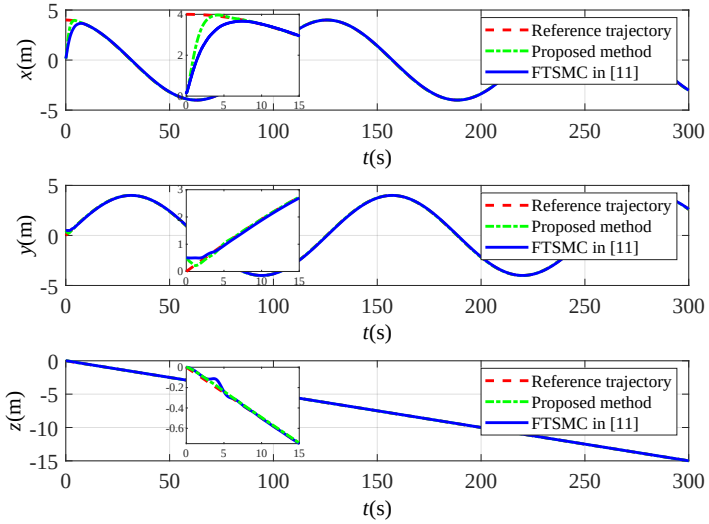

Figure 4. Trajectory tracking positions comparison of the underactuated AUV.

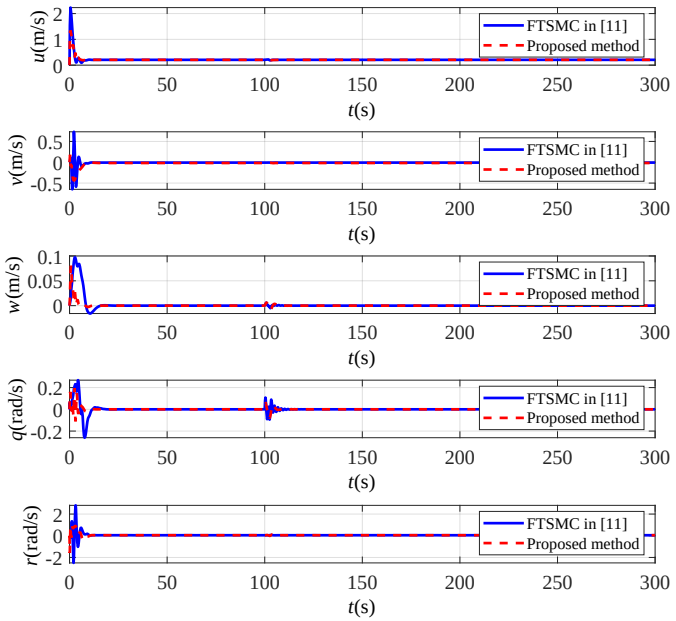

Figure 5. Trajectory tracking velocities comparison of the underactuated AUV.

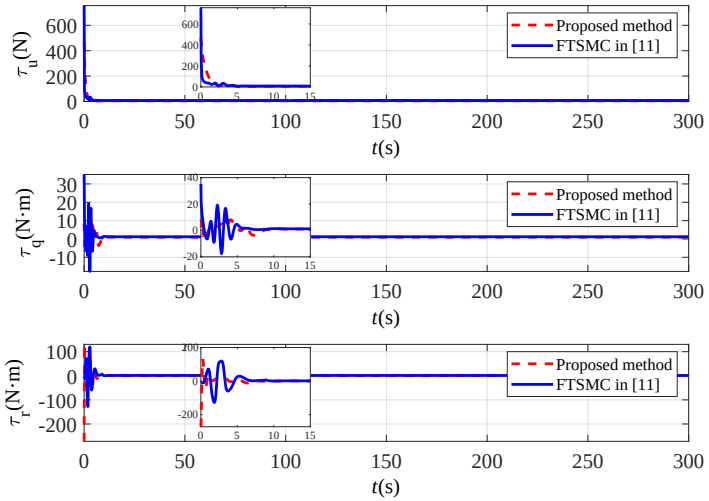

Figure 6. Control input comparison of the underactuated AUV.

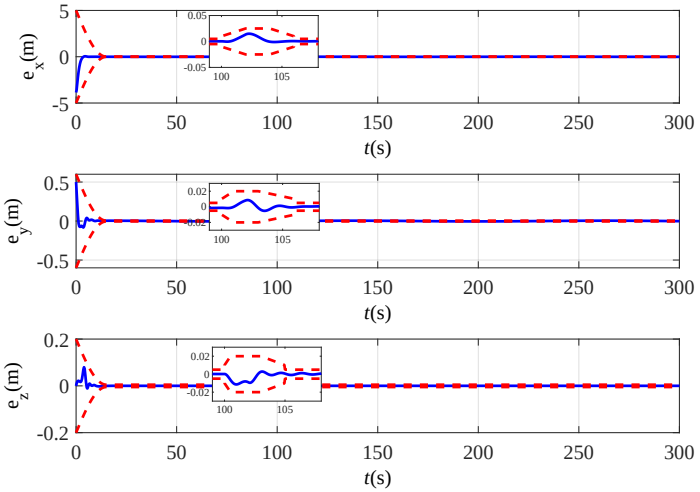

Figure 7. The position error of the underactuated AUV.

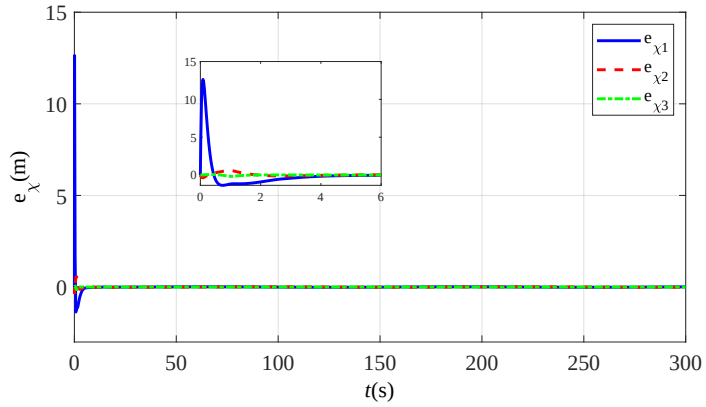

Figure 8. The approximation error of the lumped disturbance χ.

5. Conclusions

This paper has investigated the trajectory tracking issue for underactuated AUV under uncertain dynamics and additional disturbances. The FXTNTSMC strategy based on adaptive RBFNN and flexible prescribed performance has been proposed. The flexible PPC incorporates a risk monitoring mechanism that proactively adjusts performance boundaries to prevent instability and singularity. The control scheme ensures that the position error achieves to a bounded region within a fixed time independent of initial conditions. The adaptive RBFNN can effectively approximate the lumped disturbance online. The proposed approaches are validated in simulation results, which demonstrated the effectiveness and advantages through comparison. In future work, we will focus on extending

the proposed FXTNTSMC framework to event-triggered cooperative formation control for multiple underactuated AUVs [31], thereby effectively reducing communication and computation burdens under limited bandwidth in practical ocean environments.

Author Contributions

G.F.: conceptualization, methodology, writing—original draft preparation; Y.Z.: supervision, conceptualization, writing—reviewing and editing; S.Y.: data curation, validation, formal analysis. All authors have read and agreed to the published version of the manuscript.

Funding

This work was supported in part by the National Natural Science Foundation of China under Grant 62373072, 62073054, and 62003070. The Postdoctoral Natural Science Foundation with grant number 2024M764265.

Data Availability Statement

The authors confirm that the data supporting the findings of this study are available within the article.

Conflicts of Interest

The authors declare no conflict of interest.

Use of AI and AI-Assisted Technologies

No AI tools were utilized for this paper.

References

1. Zhao, W.; Xia, Y.; Zhai, D.; et al. Event-Triggered Formation Control of Unknown Autonomous Underwater Vehicles Subject to Arbitrarily Large Time-Varying Communication Delays. *IEEE Trans. Veh. Technol.* **2025**, *74*, 3901–3912.
2. Lin, C.; Zhang, Y.; Han, G.; et al. Multiple Autonomous Underwater Vehicles-Assisted Data Collection in 6G-Driven Underwater Wireless Networks Based on Software-Defined MARL. *IEEE Trans. Intell. Transp. Syst.* **2025**, *26*, 17928–17939.
3. Yu, L.; Qiao, L.; Shen, C. High-Speed Obstacle Avoidance of a Large-Scale Underactuated Autonomous Underwater Vehicle Under a Finite Field of View. *IEEE Trans. Autom. Sci. Eng.* **2025**, *22*, 1996–2005.
4. Cao, Z.; Fan, H.; Hu, X.; et al. Complete Coverage Search for Multiple Autonomous Underwater Vehicles Based on Neuronal Activity Reassignment. *IEEE Trans. Intell. Transp. Syst.* **2025**, *26*, 9693–9710.
5. Wang, M.; Juan, R.; Li, Z.; et al. Formation Control and Intention Compensating of AUVs Using Multi-Agent Reinforcement Learning and Predict Network. *Ocean Eng.* **2025**, *342*, 122854.
6. Wang, J.; Li, T. Guest Editorial Special Issue on AI-Powered Planning and Control of Autonomous Marine Vehicles. *IEEE Trans. Syst. Man Cybern. Syst.* **2025**, *55*, 2–3.
7. Xi, M.; Wen, J.; He, J.; et al. An Expert Experience-Enhanced Security Control Approach for AUVs of the Underwater Transportation Cyber-Physical Systems. *IEEE Trans. Intell. Transp. Syst.* **2025**, *26*, 14086–14098.
8. Wang, J.; Cui, H.; Xu, H.; et al. Protocol-Based Dissipative Consensus Formation Control for Multi-AUVs with Transmission Delays. *IEEE Trans. Veh. Technol.* **2025**,*75*, 7078–7090.
9. Wang, Z.; Wen, J.; Xi, M.; et al. An Information-Interdependence Deep Reinforcement Learning Path Planning Scheme for AUV with Ocean Currents Utilization. *IEEE Trans. Veh. Technol.* **2026**, *75*, 3816–3828.
10. Wang, X.; Xu, B.; Guo, Y. Minimum Error Entropy Robust Delay Filter for Multi-AUV Cooperative Localization. *IEEE/ASME Trans. Mechatron.* **2025**, *30*, 1567–1577.
11. Ali, N.; Tawiah, I.; Zhang, W.; et al. Finite-Time Extended State Observer Based Nonsingular Fast Terminal Sliding Mode Control of Autonomous Underwater Vehicles. *Ocean Eng.* **2020**, *218*, 108179.
12. Xia, G.; Zhang, Y.; Zhang, W.; et al. Robust Adaptive Super-Twisting Sliding Mode Formation Controller for Homing of Multi-Underactuated AUV Recovery System with Uncertainties. *ISA Trans.* **2022**, *130*, 136–151.
13. Hou, Y.; Jin, X.; Qin, J. Adaptive RBFNN-Based Fixed-Time Event-Triggered Control of a Class of Disturbed Euler-Lagrange Systems with Actuator Faults. *J. Franklin Inst.* **2025**, *362*, 108116.
14. Long, H.; Zhang, P.; Guo, T.; et al. Saturated Adaptive Fuzzy Fixed-Time Nonsingular Integral Terminal Sliding-Mode Control of AUVs. *IEEE Trans. Cybern.* **2025**, *55*, 1634–1647.
15. Zhang, P.; He, X.; Yu, J. A Distributed Fixed-Time Neurodynamic Algorithm and Its Application in Multi-Autonomous Underwater Vehicle Collaborative Escorting. *IEEE Trans. Netw. Sci. Eng.* **2025**, *12*, 4140–4151.
16. Li, X.; Qin, H.; Li, L.; et al. Fixed-Time Velocity-Free Safe Formation Control of AUVs with Actuator Saturation and Unknown Disturbances. *Ocean Eng.* **2023**, *285*, 115361.

17. Su, B.; Wang, H.; Wang, Y. Dynamic Event-Triggered Formation Control for AUVs with Fixed-Time Integral Sliding Mode Disturbance Observer. *Ocean Eng.* **2021**, *240*, 109893.
18. Li, J.; Du, J.; Li, Y.; et al. Distributed Robust Prescribed Performance 3-D Time-Varying Formation Control of Underactuated AUVs Under Input Saturations and Communication Delays. *IEEE J. Ocean. Eng.* **2023**, *48*, 649–662.
19. Wang, W.; Wen, T.; He, X.; et al. Path Following with Prescribed Performance for Underactuated Autonomous Underwater Vehicles Subjects to Unknown Actuator Dead-Zone. *IEEE Trans. Intell. Transp. Syst.* **2023**, *24*, 6257–6267.
20. Chen, G.; Dong, J. Approximate Optimal Adaptive Prescribed Performance Fault-Tolerant Control for Autonomous Underwater Vehicle Based on Self-Organizing Neural Networks. *IEEE Trans. Veh. Technol.* **2024**, *73*, 9776–9785.
21. Wang, Y.; Yang, Y.; Li, Y.; et al. Fixed-Time Prescribed Performance Control for Trajectory Tracking of Underactuated AUVs Under Thrust Saturation. *Ocean Eng.* **2026**, *344*, 123455.
22. Zhang, H.; Hu, Y.; Song, Z. Event-Triggered Adaptive Fault-Tolerant Control with Pre-Specified Performance for AUVs Trajectory Tracking. *Ocean Eng.* **2024**, *313*, 119372.
23. Shi, Y.; Xie, W.; Zhang, G.; et al. Event-Triggered Quantitative Prescribed Performance Neural Adaptive Control for Autonomous Underwater Vehicles. *IEEE Trans. Syst. Man Cybern. Syst.* **2024**, *54*, 3381–3392.
24. Liu, H.; Huang, H.; Tian, X.; et al. Distributed Optimal Formation Control for UAV-USV Multiagent Systems: A FEWNN-Based RL Approach with Self-Adjusting Prescribed Performance. *Ocean Eng.* **2026**, *353*, 124707.
25. Wang, Y.; Wang, H.; Zhu, J.; et al. Flexible Prescribed Performance-Based Approaching Control for UAV Aerial Recovery Under Multiwind Disturbances. *Chin. J. Aeronaut.* **2025**, *38*, 103282.
26. Guan, Y.; Xia, Y.; Geng, Z.; et al. Unified Flexible Prescribed Performance Control for Actuator-Constrained Systems Through an Event-Triggered Mechanism. *Chaos Solitons Fractals* **2025**, *201*, 117216.
27. Ba, D.; Li, Y.; Tong, S. Fixed-Time Adaptive Neural Tracking Control for a Class of Uncertain Nonstrict Nonlinear Systems. *Neurocomputing* **2019**, *363*, 273–280.
28. Deng, H.; Krstić, M. Stochastic Nonlinear Stabilization I: A Backstepping Design. *Syst. Control Lett.* **1997**, *32*, 143–150.
29. Zuo, Z. Nonsingular Fixed-Time Consensus Tracking for Second-Order Multi-Agent Networks. *Automatica* **2015**, *54*, 305–309.
30. Lei, J.; Meng, T.; Li, D.; et al. Switched Hybrid Control for Spacecraft Attitude Control with Flexible and Guaranteed Performance. *IEEE Trans. Control Syst. Technol.* **2025**, *33*, 582–596.
31. Chen, C.; Zou, W.; Xiang, Z. Event-Triggered Connectivity-Preserving Formation Control of Heterogeneous Multiple USVs. *IEEE Trans. Syst. Man Cybern. Syst.* **2024**, *54*, 7746–7755.